Article

Mobility and Location of Drainage Divides Affected by Tilting Uplift in Sado Island, Japan

Akimasa Sakashita[1], Noritaka Endo[1,*]

[1] Department of Earth Sciences, Graduate School of Natural Science & Technology, Kanazawa University, Kanazawa, Ishikawa, 920-1192, Japan; sakaxtusii@gmail.com

* Correspondence: wisteria@staff.kanazawa-u.ac.jp

Abstract: Drainage divide is a dynamic feature that migrates in response to tectonic activity. The asymmetric uplift between two adjacent basins causes the divide migration from a slower to faster uplift area. Sado Island, Japan, has been affected by southeastward tilting uplift since ca. 300k years. Despite the faster uplift on the northwest, the main divides have existed on the southeast side of the geometric center of the island, with no other feature suggesting tectonic inversion of the tilting direction. In this study, we conducted a DEM-based investigation that focused on divide migration. A spectrum from very inactive to active divide migration in the northwest. Regardless of their position, actively migrating divides are comprehensible, but inactive divides located in a relatively slow uplift area remain unclear. We concluded that some divides slowed down owing to the local balance of erosion rates across the divides, not implying the balance between uplift and river erosion at the basin scale, reflecting disequilibrium in river longitudinal profiles. The main divides of Sado have presumably continued to slowly migrate toward the faster uplift area; however, they are most likely to have never overcome the moving geometric center owing to land expansion at the seacoast due to asymmetric uplift.

Keywords: Sado Island; divide migration; tilting uplift; stream capture; geomorphic indexes; topographic analysis

1. Introduction

The drainage divide has been recognized as a dynamic geomorphological feature that moves in response to several factors. Because divide migration has a significant impact on landform development, causing changes in the drainage area, sediment supply, and river flow discharge, it has been progressively studied in association with drainage networks and landform changes [1]. The direction of divide migration is determined, on a short timescale by the difference in erosion rates across the divide (divide moves from a faster eroded basin to a slower eroded basin) [1]. However, it can be influenced by other factors, such as spatially asymmetric uplift [2–6], differences in the erodibility of rocks across the divide [7–9], and crustal horizontal advection due to tectonics [2,10–11]. The basin landscape is affected by elevation changes due to the balance of uplift and erosion; therefore, the change in uplift rate distribution modifies not only long-term and large-scale landscapes but also local landscapes. Asymmetric uplift between two adjacent basins plays an important role in landslide generation, particularly, in regions with active tectonics [12]. Previous studies reported that, in cases of asymmetric uplift, the main divide moved from a slower uplift basin to a faster uplift basin, and observed a linear correlation between the differences in erosion rate and the divide migration rate, eventually reaching a quasi-steady state during asymmetric uplift [10–11,13]. Although several recent studies on natural landforms affected by asymmetric uplift have been conducted to elucidate the history of landform formation processes along with divide migration [3,14–16], further research is required for a deeper understanding of divide migration affected by asymmetry or heterogeneous uplift.

Preprints (www.preprints.org) | NOT PEER-REVIEWED | Posted: 26 December 2022 doi:10.20944/preprints202212.0473.v1

Sado Island, located in the Sea of Japan near Honshu Island (the largest island in Japan), is a tectonically active area. Sado Island is composed of two elongated portions, Osado and Kosado, both of which extend almost parallelly northeast to southwest (Figure 1). The island is affected by southeastward tilting uplift (uplift rate is faster on the northwestern side than on the southeastern) in both Osado and Kosado, which can be confirmed from the heights of marine terraces showing the former shoreline level [17–19]. The main divides extend along the longitudinal direction of Osado and Kosado. At present, Sado exhibits unexpected aspects regarding the position of the main divides. In the case of an equilibrium state of balance between the incision and uplift rates, according to the stream power model, in which the slope exponent is generally larger than the area exponent, the longitudinal profile of a river in a basin being uplifted faster should be steeper than that in a basin being uplifted slower. Thus, based on this understanding, the position of the divide should be on the faster uplifted side of the geometric center of the land; that is, short steep rivers occur on the faster uplifted side, whereas long gentle rivers occur on the slower uplifted side [15]. In Sado Island, however, despite the faster uplift on the northwestern side than on the southeastern side, each main divide is located on the southeastern side of the geometric center of Osado and Kosado. Ota [19] interpreted this occurrence as a change in direction of the tilting uplift, and that the present situation is transitional in which the divides actively migrate toward the northwest, adjusting to the modern direction of tilting, although the tectonic inversion has not been evident thus far. In this study, we elucidate the developmental process of the landform of Sado Island to understand the modern state of the divides (divide mobility), based on geomorphological analysis using geographical information system (GIS) data, as case studies of divide migration affected by asymmetric uplift remain scarce.

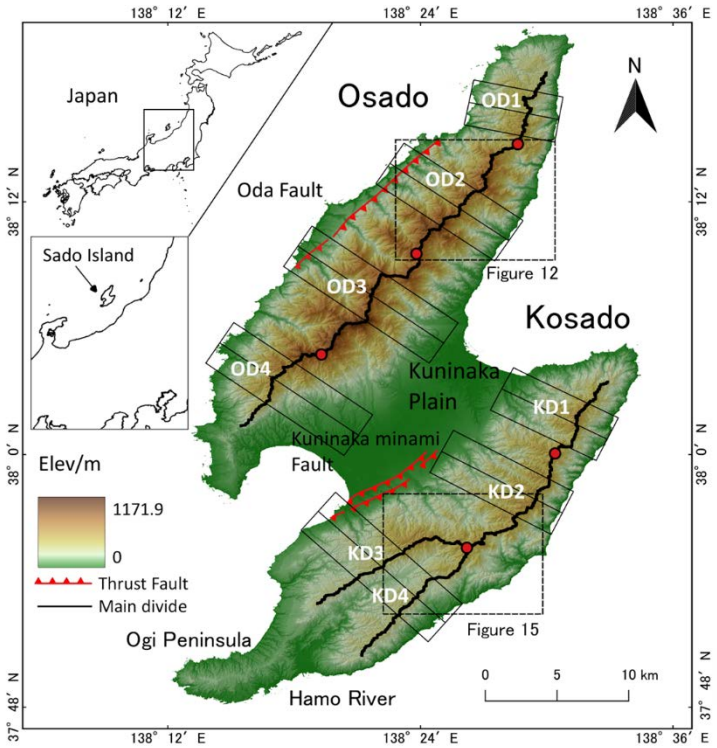

Figure 1. Topographic map of Sado Island. The thick black lines represent the main divides. The divides are segmented for analysis, and the segments are termed as OD1–4 in Osado and KD1–4 in Kosado, respectively. The boundaries of segments are indicated by red circles. Seven black thin boxes with a longitudinal center line show ranges to create swath profiles (Figure 7). The locations of currently identified active faults are also shown. This map follows the GSI 1:200,000 Seamless Geological Map of Japan (V2 Shapefile National Version Revised).

 doi:10.20944/preprints202212.0473.v1

2. Study Area

Sado Island, located across the Mogami Trough from Honshu Island (Figure 1), has an area of approximately 857 km². Sado Island is composed of two parts, Osado and Kosado, which have an elongated shape from north to south and are connected by a sedimentary plain (the Kuninaka Plain). Excluding the Kuninaka Plain, Sado Island consists primarily of Tertiary sedimentary and volcanic rocks, such as dacite and andesite (Figure 2) and displays an overall NE-SW oriented trend [20,21]. The volcanic rocks on Sado Island are divided into five stages based on chemical composition and stratigraphy, and their eruption volumes were estimated [22]. The Aikawa Group, a compilation from the first to fourth stages, was estimated to be 22 to 18 million years old formed in the early Miocene, and the Tsuruko and Nakayama Formations, a part of the fifth stage, were estimated to be approximately 15 to 4 million years old.

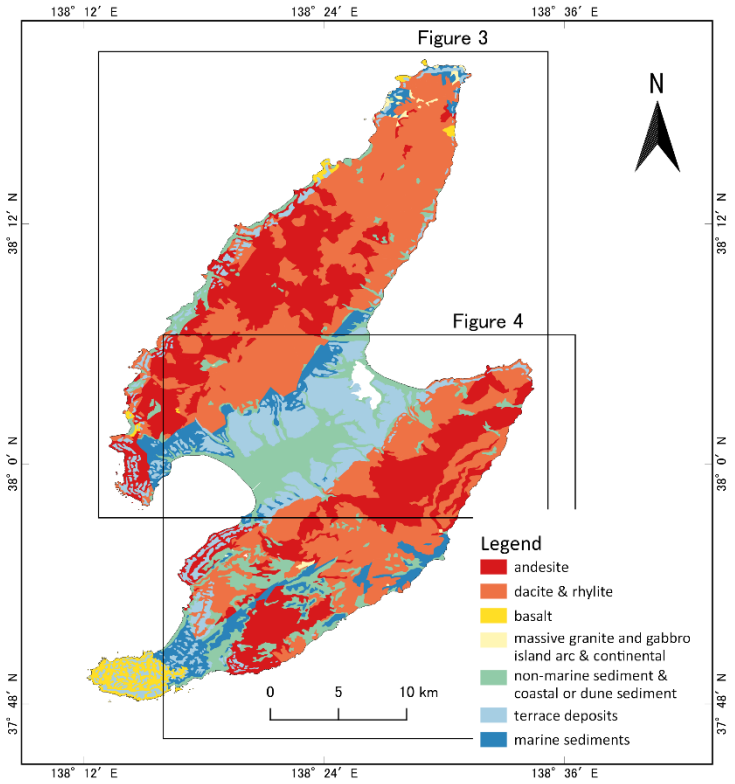

Figure 2. Geological map of Sado Island. This map follows the Seamless Geological Map of Japan 1:200,000 V2 (Geological Survey of Japan, AIST, Data updated on April 6, 2020, https://gbank.gsj.jp/seamless/) Revised. The two rectangles indicate the locations of Figures 3 and 4.

Holocene and Pleistocene marine terraces were formed on the coast of Sado Island, and uplift rates were estimated based on their formation ages. The estimation suggests tilting uplifts that has continued since at least ca. 300k years ago to the modern era, whose uplift rate is faster on the northwestern side of both Osado and Kosado [19]. The tilting directions are N125°E in Osado and N110°E in Kosado. The tilting speeds along the axes are 0.06 m/1000 m/1000 y on Osado and 0.02 m/1000 m/ 1000 y on Kosado. The maximum uplift rates are 1.1 m/1000 y for Osado and 0.9 m/1000 y for Kosado [18]. The tilting uplift is considered to be caused by a compressive stress field with a compressive axis in the northwest to southeast direction around Sado Island, which formed the active Oda fault on Osado and the Kuninaka-minami fault on Kosado [19,23].

Both Osado and Kosado have two mountain ridges, with highest elevations of 1171.9 m and 645.8 m in Osado and Kosado, respectively. The main drainage divides extend ap-

 doi:10.20944/preprints202212.0473.v1

proximately parallel to the longitudinal direction of Osado and Kosado. Although the position of the main divide from the central to southern areas of Osado (OD2-4 in Figure 1) is almost on the central axis of Osado, that in the northern area deviates toward the east (OD1 in Figure 1). The main divide from the north to the central areas of Kosado (KD1-2 in Figure 1) is biased eastward from the central axis of Kosado, whereas in the southern area (KD3-4 in Figure 1), the divide ridge separates into two. The Hamo River flows between the two divide-branches in a southwesterly direction, forming an alluvial lowland.

We excluded the Ogi Peninsula from the study area, located at the southern end of Kosado (Figure 1), because it shows a different tendency of spatial distribution of marine terrace height than those in other areas of Kosado [17–19]. This suggests that the uplift rate in the Ogi Peninsula is faster on the southern side than on the northern side, that is, it displays an opposite tilting uplift direction to that of other areas of Sado. In terms of geology, the Ogi Peninsula implies independent tectonic activity in other areas of Sado Island: the Ogi Peninsula is composed of basalt, whereas other areas consist of dacite and andesite [18,24] (Figure 2). In addition, the Ogi Peninsula has a small area and low elevation in comparison with those of other places; therefore, it is excluded from the present target area.

3. Method

3.1. Datasets

Geomorphological analysis was conducted based on a Digital Elevation Model (DEM). The data used for Sado Island are the 10 m mesh DEM provided by the Geospatial Information Authority of Japan (GSI: the Geographical Survey Institute) (https://fgd.gsi.go.jp/download/terms.html) and the 1:200,000 Japan Geological Map provided by the Geological Survey of Japan.

In the analysis, we partitioned Sado Island into four sections for both Osado and Kosado for clear comparison between both sides across the main divides. Portioning was based on the elevations of the main divides, and each segment is hereafter referred to as OD1, OD2, OD3, and OD4 in Osado and KD1, KD2, KD3, and KD4 in Kosado (Figure 1).

3.2. Longitudinal Profile and Normalized Steepness Index (k_{sn})

In consideration of the development of bedrock rivers, the stream power incision model (SPIM) is commonly used, in which the incision rate of downward cutting is a function of the contributing drainage area (as a proxy for water discharge) and riverbed slope. The differential equation for the temporal change of riverbed elevation related to a balance between the uplift rate and incision rate is therefore expressed along with SPIM as follows [25]:

$$\frac{\partial z}{\partial t} = U - KA^m S^n, \tag{1}$$

where z is the elevation of the riverbed; t is the time; U is the bedrock uplift rate; A is the upstream contributing area; S is the channel gradient; m and n are empirical exponents; and K is an erosion constant that depends on bedrock erodibility and precipitation [26,27]. Assuming that the erosion constant is uniform, Equation (1) for rivers in equilibrium can be rewritten as follows:

$$S = k_s A^{-\theta}, \tag{2}$$

$$k_s = \left(\frac{U}{K}\right)^{\frac{1}{n}}, \tag{3}$$

$$\theta = \frac{m}{n}, \tag{4}$$

 doi:10.20944/preprints202212.0473.v1

where k_s is the steepness index and θ is the concavity index. The steepness index, k_s, was used to compare the steepness among different rivers. The value of the actual slope of riverbeds is not constant even along an identical channel (it decreases from upstream to downstream); therefore, for comparison of steepness with other rivers, the steepness index is used as a representative value for each river. The steepness index can be obtained with the gradient of the regression line in a logarithmic plot of S vs. A based on geomorphological data using Equation (2). This method is easy to implement, but the values obtained from the regression often vary widely among different rivers, owing to the noise of natural field data, when both k_s and θ are simultaneously determined from the regression analysis. Fixing the concavity index at a certain plausible value prior to the regression is a viable solution. The value of the concave index, θ, generally has a range of 0.4–0.5 [26,27], and many previous studies had therefore adopted 0.45 as a fixed value of the concavity index, to obtain the steepness indices from regression [5,14,29–30], where those obtained are termed as the normalized steepness index (k_{sn}). This study also adopted 0.45 as the concavity index. To detect flow paths and then determine k_{sn}, as well as to make swath profiles, we used the TopoToolbox [31]. To detect flow paths, we set the threshold of the drainage area to 4000 m² by conforming the results to the GSI map. The knickpoints were detected using the knickpointfinder function. The constrained regularized smoothing (CRS) method of Schwanghart [32] was used for the detected channels as preprocessing for the calculation of k_{sn}, with the CRS set to K = 5.

3.3χ. Parameter

Assuming an equilibrium between the uplift and erosion rates in Equation (1), or Equation (2), by integrating with respect to distance, x, from downstream to upstream, we obtain:

$$z(x) = z_b + \left(\frac{U}{KA_0^m}\right)^{\frac{1}{n}} \chi, \tag{5}$$

$$\chi = \int_{x_b}^{x} \left(\frac{A_0}{A(x)}\right)^{\theta} dx, \tag{6}$$

Where z_b is the elevation at $x = x_b$; and A_0 is the scaling value. χ is a parameter of virtual distance that accounts for the change in drainage area along a channel, as defined in Eq. (6), and is proportional to the riverbed elevation of an ideal graded river (equilibrium river). When a river reaches equilibrium, elevation $z(x)$ is a linear function of χ, as shown in Equation (5). The deviation of $z(x)$ from linearity with χ indicates a disequilibrium of the river landform. Therefore, if the values of χ at a valley head are equal across a divide, the divide is interpreted as being in a steady state [1]. When χ values differ across the divide, a potential instability of the divide exists because the χ gap indicates the difference in the extent of landform development between basins. A process of topographic change is assumed such that the values of χ become similar across the divide, and divide migration is expected from the site with a higher χ to the site with a lower one [1]. In the present study, χ was calculated using the TopoToolbox of MatLab's library [31]. To avoid the influence of sedimentation in the Kuninaka Plain (alluvial plain), the starting point for the integration of Equation (5) was set to an elevation of 70 m. The m/n value of the calculated χ is 0.45 [5,14,29–30], the same as that used to calculate k_{sn}.

3.4 Gilbert Metrics

As stated above, the difference in χ values across a divide is commonly used as an indicator of divide migration [1]. However, Forte and Whipple [13] stated that, in the case of heterogeneous uplift and/or lithology, discordance of χ across a divide can indicate a possible divide instability, but does not necessarily reflect the current divide mobility.

 doi:10.20944/preprints202212.0473.v1

They proposed Gilbert metrics (assessment using channel head elevation, local relief, and gradient) as indicators of the direction of divide migration in the case of non-uniform uplift rates. Gaps in the values of these indices across the divide arise when the erosion rate is different over the divide, and the divide moves to the side with a higher channel head elevation, higher local relief, and lower gradient. Through numerical simulations, Forte and Whipple [13] showed that all Gilbert metrics were linearly correlated with the migration rate of the divide in the case of asymmetric uplift for two adjacent basins.

To calculate the Gilbert metrics, we used DivideTools [13], where the radius of the circular window centered at the source point was set to 250 m. The relief in the Gilbert metrics is defined as the difference in elevation between the river source and the highest elevation within the circular window, and the gradient in the Gilbert metrics is defined as the average gradient between the river source point and the highest site within the window [13].

3.5. Estimation of Divide Mobility

Because the assessment of divide mobility is more accurate if the results of χ parameters and Gilbert metrics accord with each other, the combination of the Gilbert metrics and χ has recently been increasingly used [13–14,34–35]. In the case of conflict between the results of the Gilbert metrics and χ, it is possible to interpret that the Gilbert metrics indicate the current divide mobility influenced by recent situation, and χ indicates the divide migration on a long-time scale [13]. Standardized delta plots using the above indices were drawn [13]. In the plot, $\Delta\chi$ is obtained from the difference in χ across the divides for each channel. The standardized delta plot displays the average and standard deviation of the indices to depict the side on which the divide tends to migrate. Because relief is the most reliable of the three indices [13], in the present study, we interpret a divide as migrating in a certain direction if the relief and at least one of elevation or gradient indicate the same direction. This is used unless the rest of the parameters (gradient or elevation) indicate the opposite direction (e.g., the case in which both the relief and the elevation indicate northwestward migration, but the gradient indicates being stable).

4. Results

4.1. Longitudinal Profiles and the Divide Positions

A prominent contrast exists in the longitudinal profiles between the two sides of the mountains, in the northwestern and southeastern directions, in both Osado and Kosado. A greater number of knickpoints are present in the northwestern than in the southern side (Figures 3 and 4), and several of these are slope-break types, which can be recognized from the distribution of k_{sn}, which shows large fluctuations over those knickpoints [26–27,29] (Figure 5A, C, E, G and Figure 6A, C, E, G). In contrast, channels on the southeastern side have much fewer knickpoints, and most of them are step-like types, which are identified with small fluctuations of k_{sn}. In addition, several knickpoints can be seen in the lower reaches on the northwestern side, whereas only a few knickpoints are located in the downstream reaches on the southeastern side (Figures 3 and 4). The shapes of the river profiles on the southeastern side have a tendency to be smooth and concave, unlike those on the northwestern side (Figures 5 and 6).

Preprints (www.preprints.org) | NOT PEER-REVIEWED | Posted: 26 December 2022 doi:10.20944/preprints202212.0473.v1

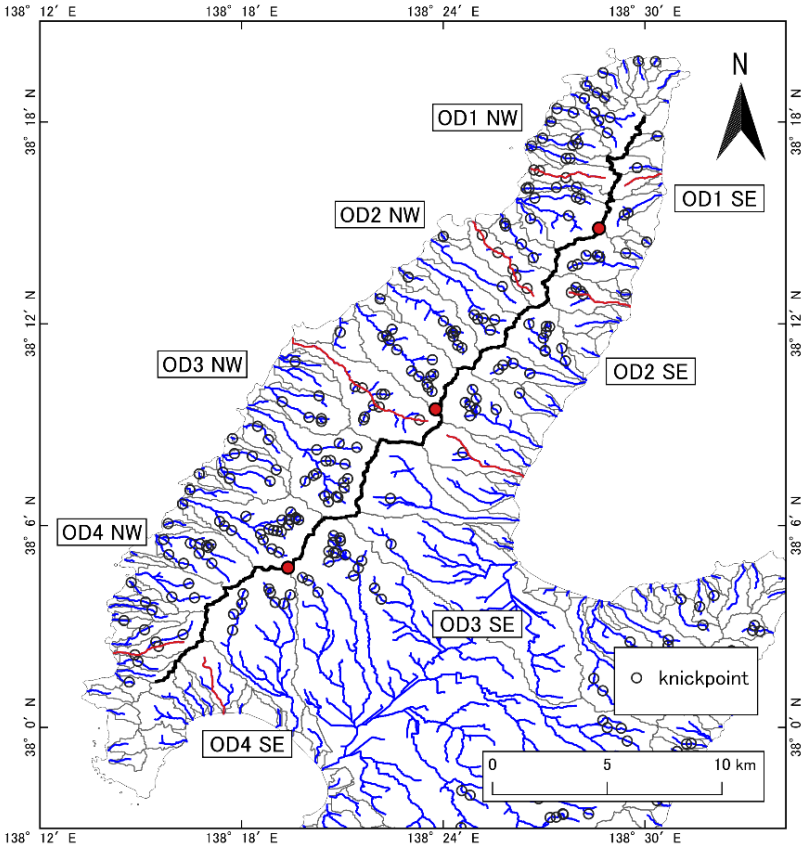

Figure 3. Location of stream channels and knickpoints in Osado. Blue and red lines indicate stream channels. Black circles represent the location of knickpoints. The red channels are representative channels in each analysis segment shown in Figure 5. Red circles are the same as in Figure 1 (boundaries of analysis segments).

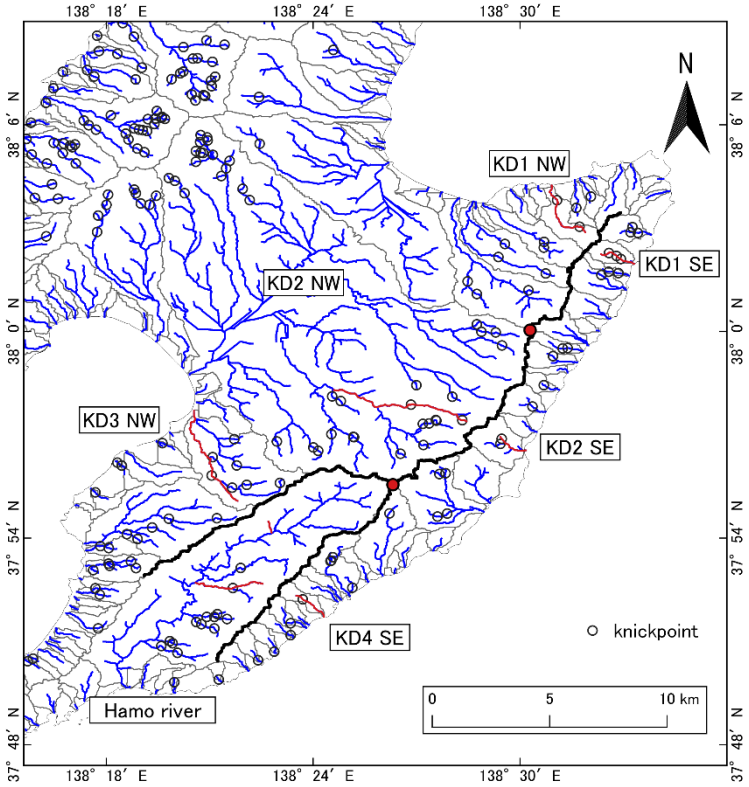

Preprints (www.preprints.org) | NOT PEER-REVIEWED | Posted: 26 December 2022 doi:10.20944/preprints202212.0473.v1

Figure 4. Location of stream channels and knickpoints in Kosado. Blue and red lines exhibit stream channels. Black circles represent the location of knickpoints. The red channels are representative channels in each segment as shown in Figure 6.

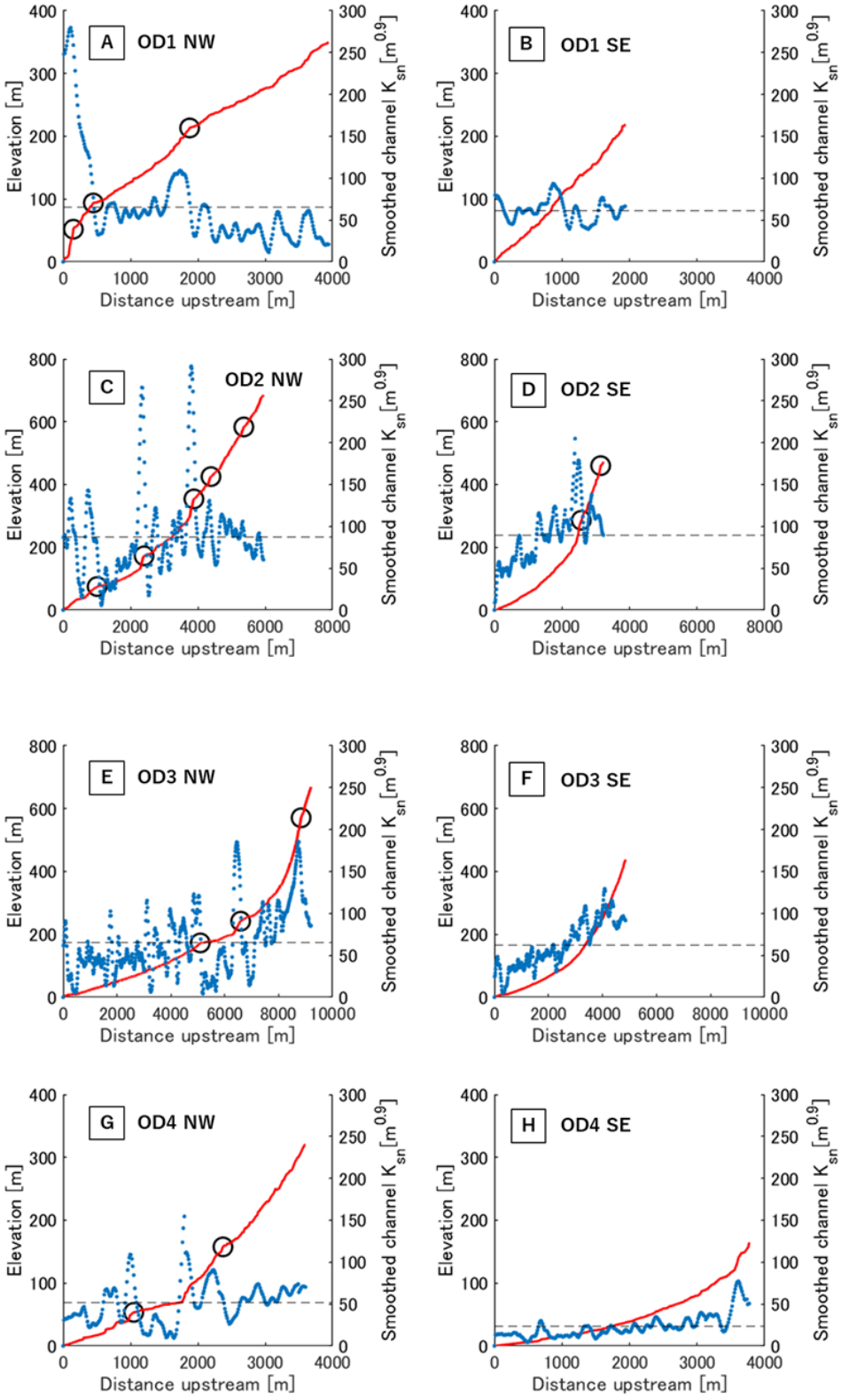

Preprints (www.preprints.org) | NOT PEER-REVIEWED | Posted: 26 December 2022 doi:10.20944/preprints202212.0473.v1

Figure 5. Representative river profiles (red lines) and knickpoints (black circles) for each analysis segment (OD1–4) in Osado, in addition to the k_{sn} values (blue dots). NW and SE indicate the northwestern and southeastern sides of the divide, respectively. Channels were selected to avoid the influence of plains and dams.

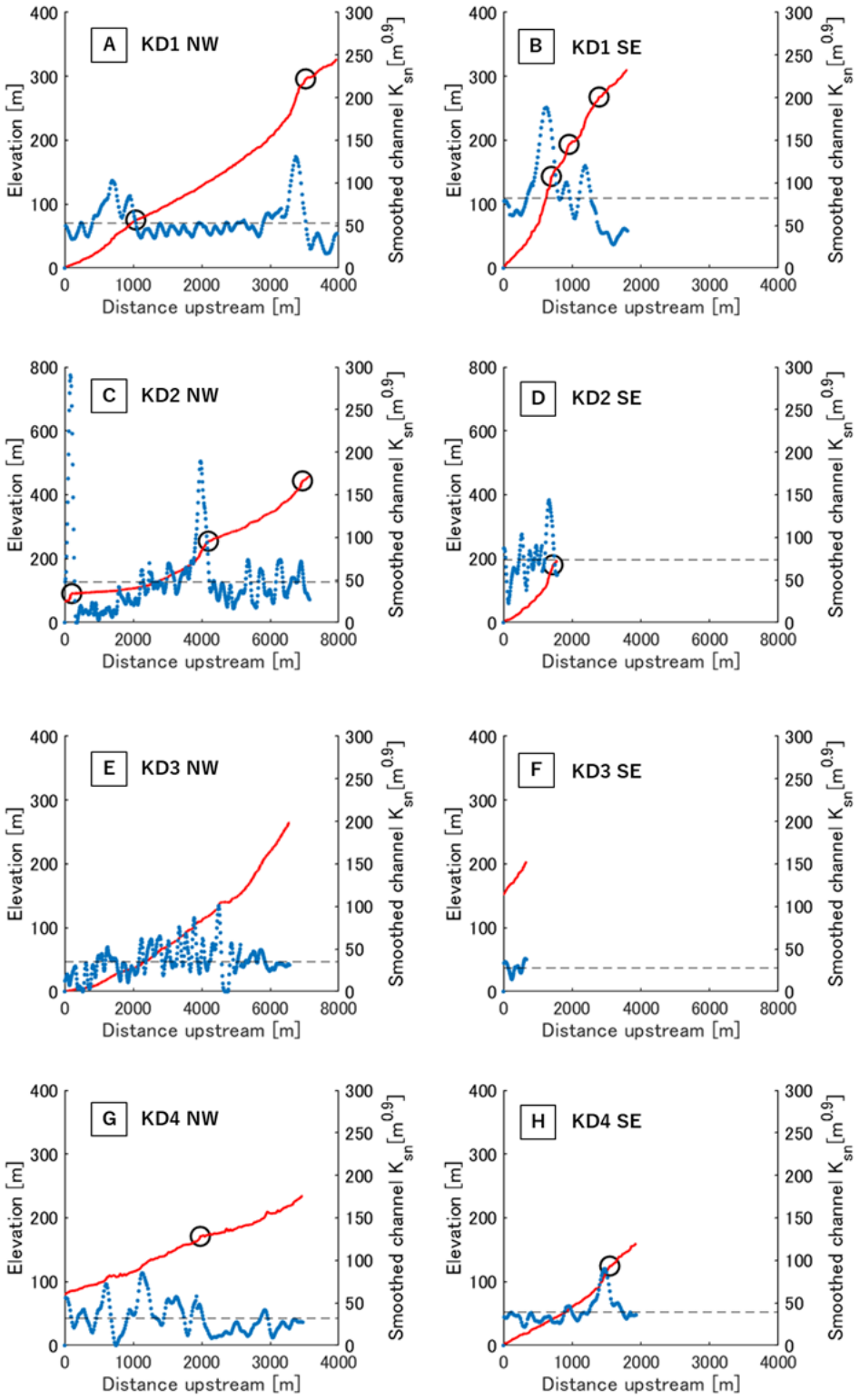

Preprints (www.preprints.org) | NOT PEER-REVIEWED | Posted: 26 December 2022 doi:10.20944/preprints202212.0473.v1

Figure 6. Representative river profiles (red lines) and knickpoints (black circles) for each segment in Kosado, in addition to the k_{sn} values (blue dots). NW and SE indicate the northwestern and southeastern sides of the divide, respectively. Channels were selected to avoid the influence of plains and dams. KD2 in (C) represents channels above 70 m in elevation to avoid the influence of plains. Rivers in (F, G) are both tributaries of the Hamo River, and shown upstream of confluences.

The distribution of river length was also asymmetrical between both sides across the divide. The swath profile (Figure 7) showed that the divides are not located on the northeastern side but rather on the southwestern side of the geometric center, despite the southeastward tilting uplift in all the segments, except for OD4 (where the alluvial plain covers the downstream reach on the southwestern side) and KD3 and 4 (where the main divide bifurcates (Figures 1 and 7G). The divides on Sado Island are therefore at unexpected positions if we consider the stable state based on SPIM.

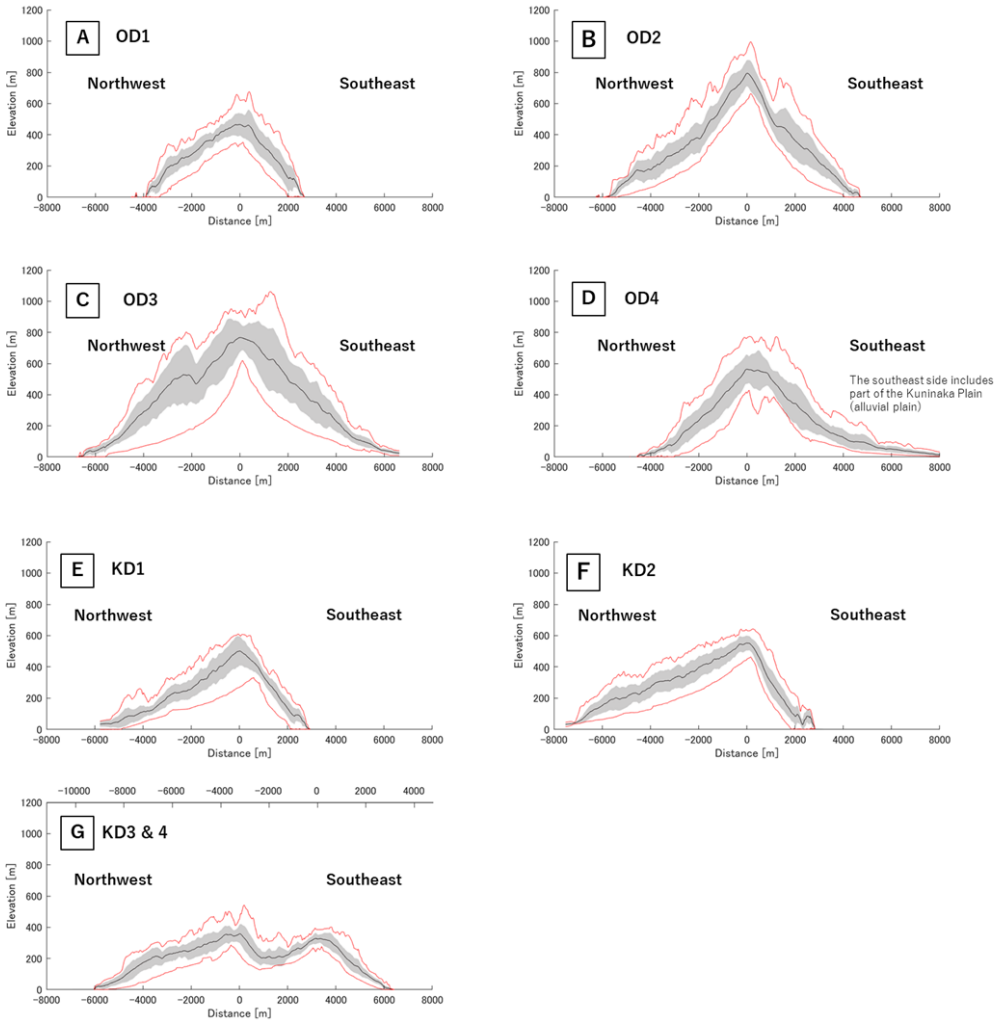

Figure 7. Swath profiles for OD1–4 and KD1–4, displaying the mean elevation on the perpendicular line to the centerline (black line), standard deviation (gray belt), and the maximum and minimum elevations (red lines). The origin of the horizontal axis is aligned with the highest elevation in the mean.

4.2. Gilbert Metrics and χ

The standardized delta plots (Gilbert metrics and $\Delta\chi$) and the χ-map of Osado are shown in Figures 8 and 9, respectively. The Gilbert metrics suggested that the divide in OD1 migrates toward the northwest, because all but the elevation values showed that the

Preprints (www.preprints.org) | NOT PEER-REVIEWED | Posted: 26 December 2022 doi:10.20944/preprints202212.0473.v1

data distribution shifted northwestward, and the elevation data range also deviated almost entirely toward the northwest (Figure 8). In contrast, the divides in OD3 and 4 seem stable, because no obvious shift of the datasets of all parameters to one side appeared in the graphs (Figure 8). In OD2, however, the Gilbert metrics pointed to stability, whereas $\Delta\chi$ indicated that the divide migrates northwestward.

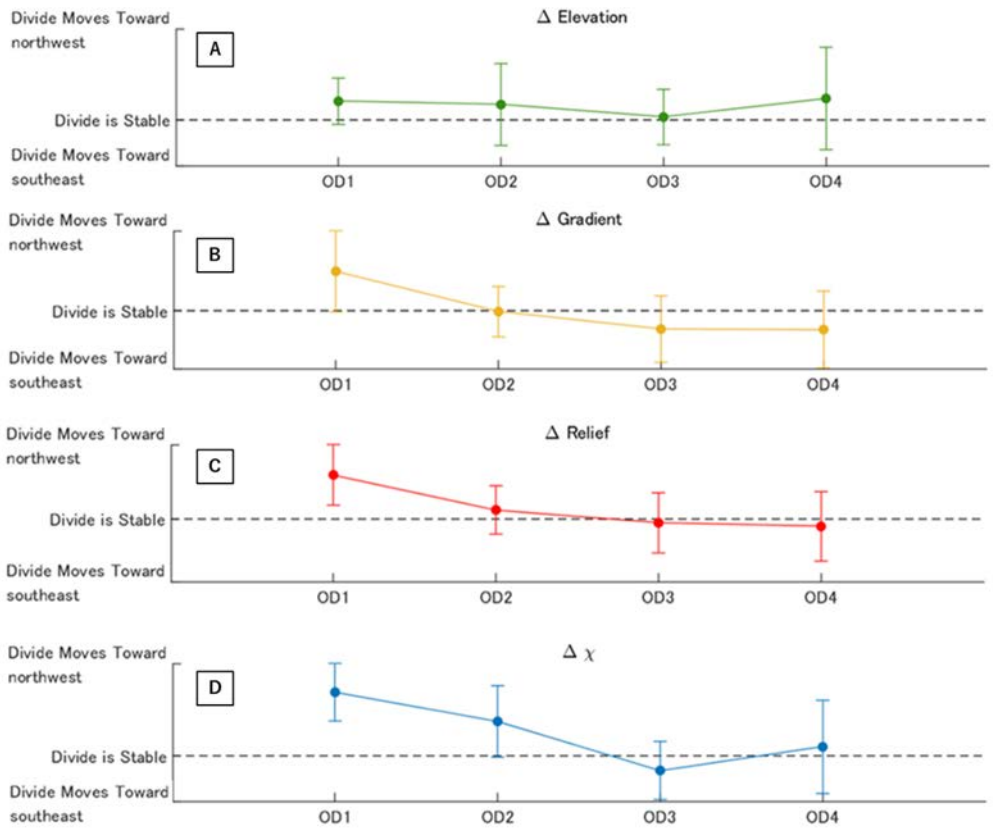

Figure 8. Standardized delta plots of Gilbert metrics and $\Delta\chi$ of each segment in Osado. (A) Elevation; (B) Gradient; (C) Relief; and (D) $\Delta\chi$. Error bars display standard deviation. These results are obtained using the DivideTools [13] based on TopoToolbox [31].

Preprints (www.preprints.org) | NOT PEER-REVIEWED | Posted: 26 December 2022 doi:10.20944/preprints202212.0473.v1

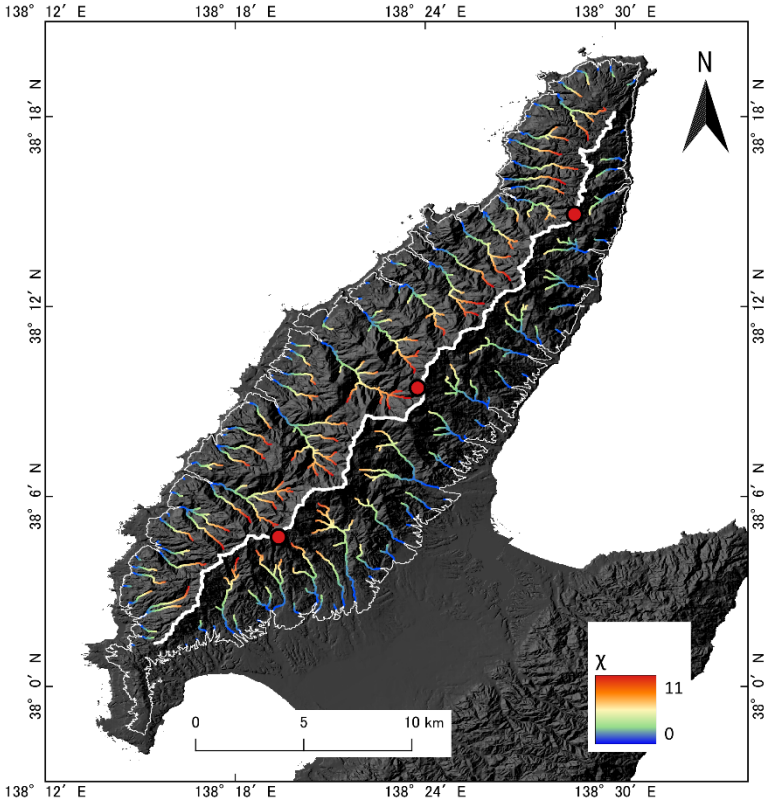

Figure 9. χ map of Osado, where the base-level was set to 70 m in elevation, to avoid the effects of alluvial plains. Thin white line indicates an elevation of 70 m, whereas the thick white line is the main divide of Osado.

The standardized delta plots and the χ map for Kosado are illustrated in Figures 10 and 11, respectively. Only KD3 showed accordance between all Gilbert metrics and $\Delta\chi$ (Figure 10), which indicates a stable divide. Among the remaining three sections, KD2 and KD4 show the accordance between $\Delta\chi$, relief and elevation suggesting northwestward divide migration, whereas the gradient indicated immobility (at least not implying the opposite migration). Based on the criterion stated in Section 3.5 the drainage divides of KD2 and KD4 are possibly migrating. In KD1, the Gilbert metrics indicated the immobility of the divide, but $\Delta\chi$ suggested migration in a northwestward direction.

Preprints (www.preprints.org) | NOT PEER-REVIEWED | Posted: 26 December 2022 doi:10.20944/preprints202212.0473.v1

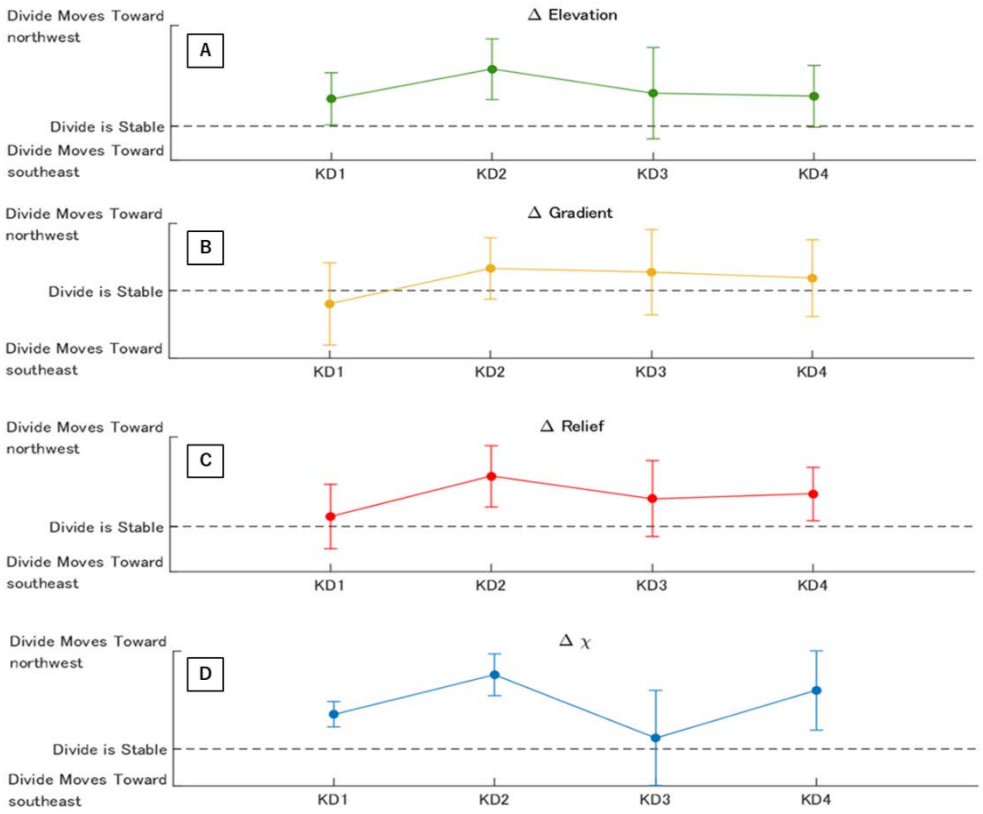

Figure 10. Standardized delta value plots of Gilbert metrics and $\Delta\chi$ for each segment in Kosado. (A) Elevation; (B) Gradient; (C) Relief; and (D) $\Delta\chi$. Error bars display standard deviation. These results are obtained using the DivideTools [13] based on TopoToolbox [31].

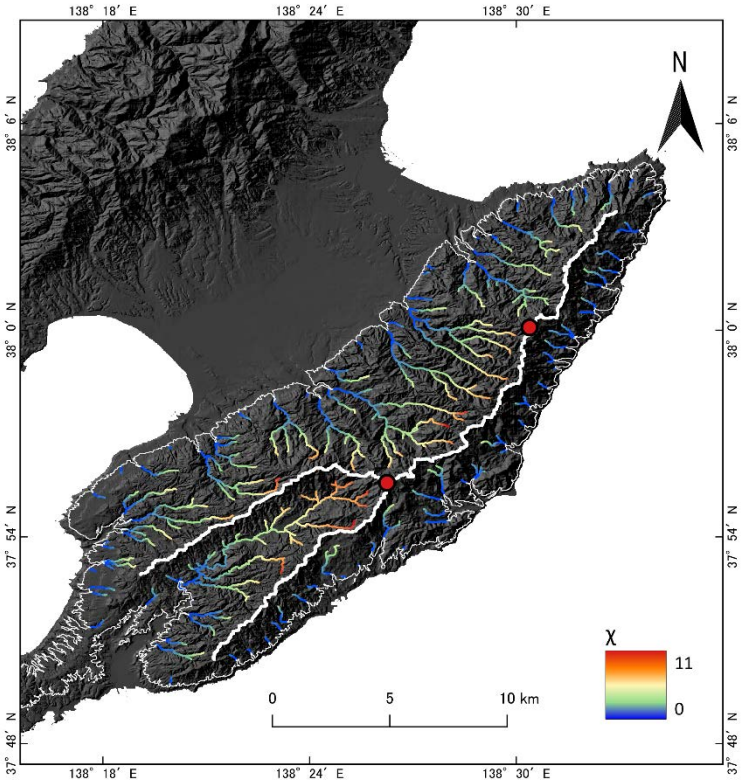

Preprints (www.preprints.org) | NOT PEER-REVIEWED | Posted: 26 December 2022 doi:10.20944/preprints202212.0473.v1

Figure 11. χmap for Kosado, where the base-level was set to 70 m in elevation, to avoid the effects of alluvial plains. The thin white line indicates an elevation of 70 m, whereas thick white line is the main divide of Kosado.

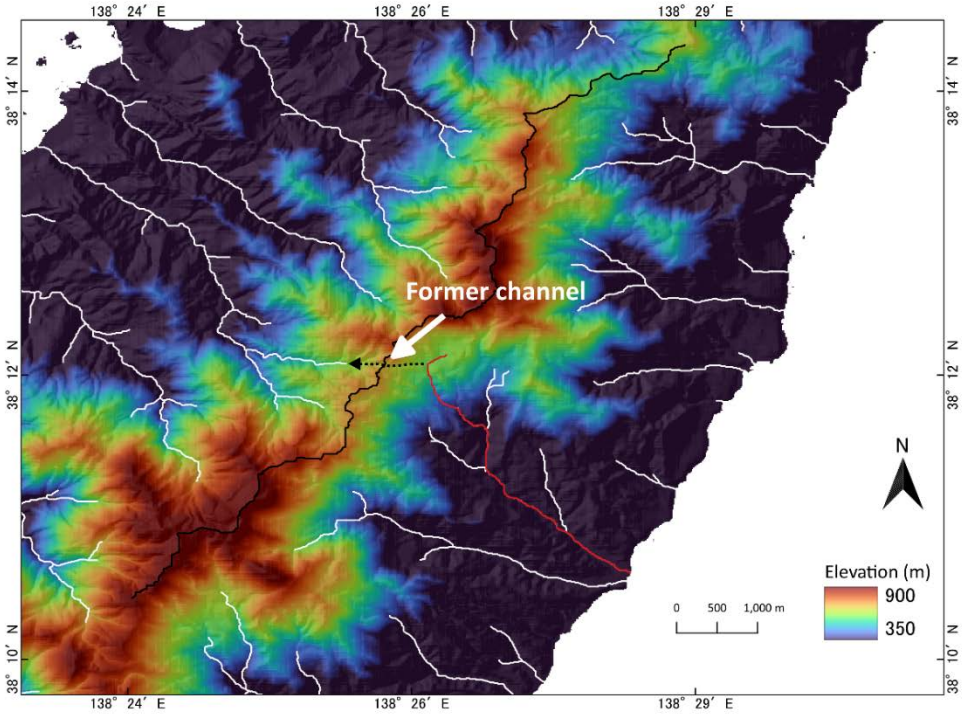

Figure 12. Location of past river capture in Osado. The red line is the river, possessing a sharp bend, that pirated the upstream reach from a river flowing on the northwestern side. The black dotted line with arrow indicates the location and flow direction of the abandoned channel, where it was connected to the front edge of the bend.

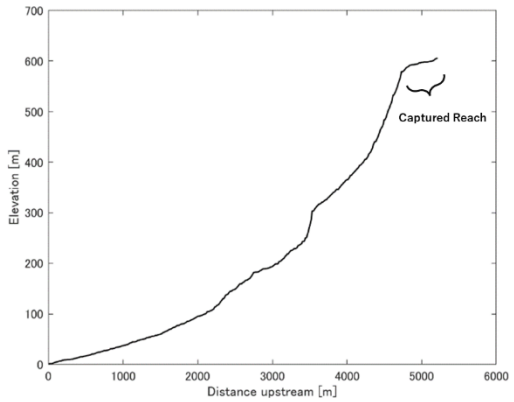

Figure 13. Profile of the river channel in Figure 12 (red line). The upstream reach with a low gradient is considered as a captured part of the river.

 doi:10.20944/preprints202212.0473.v1

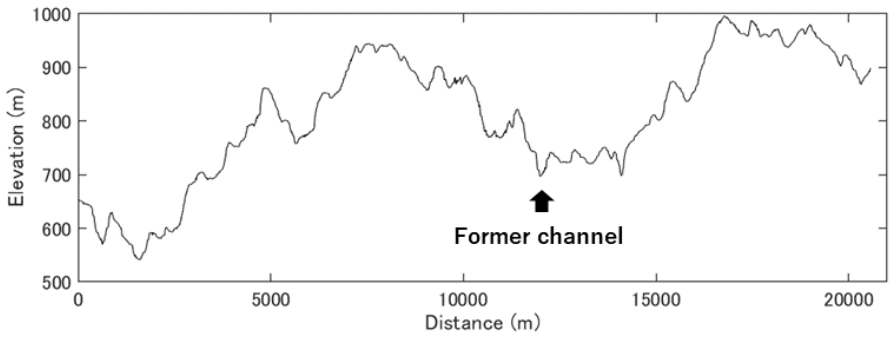

Figure 14. Elevation profile along the divide. The depression indicated by an arrow represents a region in the middle of the abandoned channel shown in Figure 12 (dotted line) and corresponds to the cross-section of the former channel prior to stream capture.

4.3 Stream Capture

In the upstream area on the southeastern side of OD2, a sharp (almost right angle) bend of the channel is present (Figure 12), where a significant change in the river profile gradient can be recognized as a knickpoint (Figure 13). A channel-like feature connects the bend to the valley head of the adjacent drainage basin across the divide. This geomorphic feature is considered as a wind-gap or abandoned channel caused by stream capture [36], which is supported by a depression of the elevation profile along the divide at the site crossing the channel-like feature that can be regarded as the cross-section of the past channel (Figure 14). Because the stream should have flowed northwestward in the abandoned channel before stream capture, the drainage divide was located southeast of the present position of the divide. Thus, it is suggested that the divide migrated from the southeast to northwest.

In Kosado, two sites considered to have undergone stream capture were identified (KC1 and KC2 in Figure 15). Similar to the case of Osado, the channels on the southeastern side of the divide have a sharp bend and noticeable slope-break in the upstream reach (Figure 16). An elevation depression, presumably a cross-section of a former channel, is shown in the elevation profile along the divide (Figure 17). Therefore, it is suggested that, similar to Osado, the divide migrated northwestward.

Preprints (www.preprints.org) | NOT PEER-REVIEWED | Posted: 26 December 2022 doi:10.20944/preprints202212.0473.v1

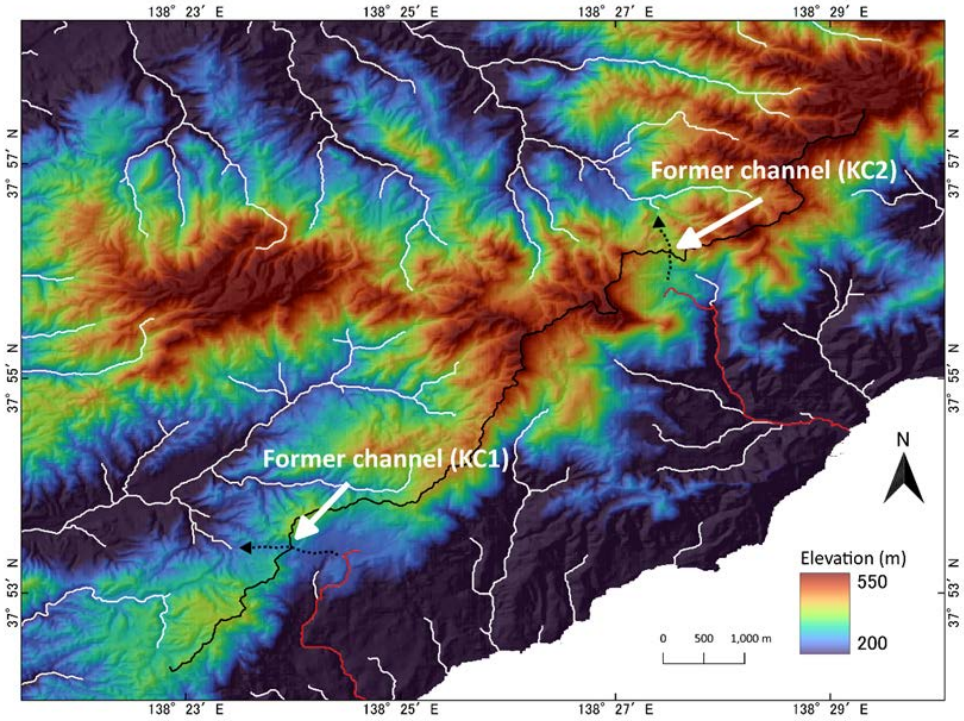

Figure 15. Locations of past river capture in Kosado. The red lines are the rivers that pirated the upstream reach from a river flowing toward northwest; and thus, had a sharp bend in the upstream reach. The black dotted lines with arrows indicate the locations and flow directions of the abandoned channels where they used to be connected to the bend reaches.

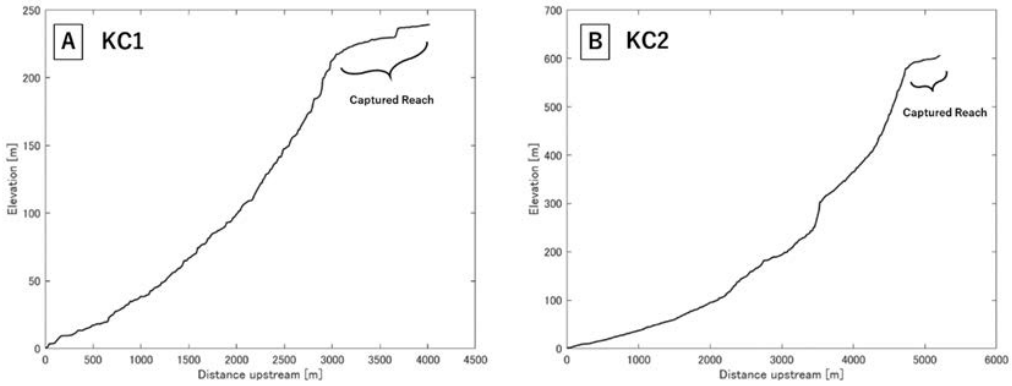

Figure 16. Profiles of rivers shown in Figure 15 as red lines. The upstream reach with a low gradient is considered as a captured part of the river.

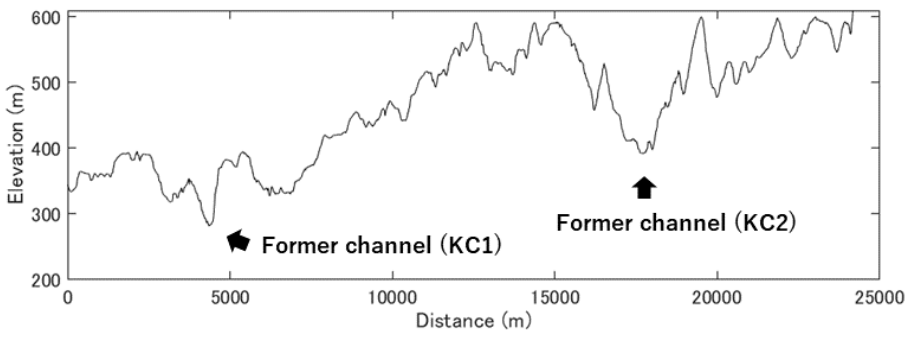

 doi:10.20944/preprints202212.0473.v1

Figure 17. Elevation profile along the divide. The depressions indicated by arrows represent a region in the middle of the abandoned channels as shown in Figure 15 (dotted lines) and correspond to the cross-sections of former channels prior to stream capture.

5. Discussion

5.1. River Topographies Affected by Tilting Uplift

In Osado, the shape of the longitudinal profile differs across the divide between the northwestern and southeastern sides (Figure 5). There are fewer knickpoints in the downstream reaches on the southeastern side than on the northwestern side. This difference is considered to originate from the tilting uplift, which shows an increase in uplift rates from the southeast to northwest. The contrast of the knickpoint type (channels on the northwestern side include many slope-break-type knickpoints) suggests the influence of transitional tectonic activity [27], which may reflect the predominance of uplift on the western coast. In Kosado, the river topographies show the effect of the tilting uplift (Figure 6). Although there are not as many knickpoints in Kosado as in Osado (probably due to suppression or screening of knickpoint formation by the Kuninaka Plain), the presence of slope-break-type knickpoints on the northwestern side of Kosado are considered to originate from tilting uplift. Thus, the river topographies on Sado Island reflect the tilting uplift of both Osado and Kosado.

Although the longitudinal profiles of the rivers on the northwestern side in all the analysis segments show the effect of tilting uplift, only OD1 exhibits a notable characteristic. The river profile on the northwestern side of OD1, with a large knickpoint near the river mouth, shows a largely convex upward shape (Figure 5). A similar convex longitudinal profile was observed under vigorous landward tilting uplift (uplift rate increases from upstream to downstream) with high uplift and precipitation rates on Yakushima Island, Japan, and according to laboratory experiments [37]. In the Himalayas of central Nepal, the Bakeya River shows convexity of the river profile resulting from a downstream increase in the uplift rate [38]. For the rivers on the northwestern side of the divide in Sado Island, southeastward tilting is the same meaning as the landward tilting. Thus, OD1 shows a stronger southeastward tilting effect than that of OD2–4. In addition, the direction of extension of the main divide in OD1 is rotated counterclockwise (north-northeast to south-southwest) and is different from those of OD2, 3, and 4 (northeast to southwest). Therefore, it is possible that the tilting uplift in Osado is complex, such that a different factor in OD1 affected the tilting than those at other places.

5.2. Divide Mobility

The results, in which both the Gilbert metrics and $\Delta\chi$ suggested migration of the divides, were obtained for OD1, KD2, and KD4 (Figures 8 and 10). Even if the divide at present is located on the southeastern side of the geometrical center (OD1 and KD2), the suggested northwestward migration of divides is comprehensible. This is because the direction accords with that predicted from SPIM, where the divides are considered to proceed toward a stable state for a southeastward tilting uplift. The divides in OD1, KD2, and KD4 likely migrate more actively than those of other places on Sado Island. In particular, for OD1, the convexity of the longitudinal profile (Section 5.1) appeared to be due to a strong disequilibrium [39], as is reflected as a markedly biased $\Delta\chi$ for OD1 (Figure 8). The disequilibrium stems from a large deviation from adjustment to the tectonic activity; thus, $\Delta\chi$ is an indicator of the difference in the extent of channel adjustment between basins across a divide on a basin scale (not limited near the divide). This is because the trunk stream gathers all the flow water in the basin, and the riverbed elevation of the trunk river determines the local base levels of all tributaries.

The Gilbert metrics are indicators of the divide mobility affected by local landform states near the divide. If their standardized delta plots suggest a steadiness of divide affected by tilting uplift, the divide motion is presumably in dynamic equilibrium with the present tectonic activity where the local erosion or denudation rates are almost equal

 doi:10.20944/preprints202212.0473.v1

across the divide. In contrast, $\Delta\chi$ relates to the extent of departure from an adjusted state of the channel network to tectonics at the basin scale. A significant value of $\Delta\chi$ (larger than standard deviation) indicates that the channels or drainage network do not entirely attain the balance between erosion and uplift; hence, the transition toward equilibrium of the entire basin is a lengthy process. The conflicting case in which the Gilbert metrics suggest a stable divide, whereas $\Delta\chi$ indicates migration is therefore acceptable and considered to reflect a dynamic (quasi-)equilibrium adjusting to the tilting uplift, while the divide position and drainage landform continue to transform over a long timescale. A previous numerical study [13] showed that, while approaching a dynamic equilibrium during tilting uplift, the migration rate of a divide decreases, and the Gilbert metrics become close to zero, whereas $\Delta\chi$ continues to rise. The divides in OD2 and KD1 correspond to this case in terms of divide mobility (Figures 8 and 10) and are considered to reflect extremely slow migration in a dynamic quasi-equilibrium, but still adjusting at the basin scale to long-time continuing tilting. However, in a previous study [13], the divide reached a position of the quasi-stable state on the faster uplift side of the geometrical center when attaining a dynamic equilibrium, unlike OD2 and KD1 which could not reach this position. The difference in the relative positions of the divide in the quasi-stable state is discussed in the next section.

The results in which both the Gilbert metrics and $\Delta\chi$ suggest a stable divide are obtained for OD3 and 4 and KD3. Among these, KD3 is in a different setup from those of OD3 and 4, because the divide in KD3 extends parallel to that in KD4 owing to the bifurcation of the divide. As the trunk river on the southeastern side of the divide in KD3, the Hamo River, flows almost parallel to the divide, we discuss only OD3 and 4. The accordant suggestion of divide stability from the Gilbert metrics and $\Delta\chi$ likely pointed to not only a local (near the divide) balance between erosion rates across the divide but also a gross balance at the basin scale. Although not on the northwestern side of the geometrical center, as expected from the southeastward tilting, the divides in OD3 and 4 are close to the geometrical center and are located relatively closer to the northwestern side in comparison with OD1 and 2, which appeared to relate to the suggested steadiness of the divides.

In Osado, the mobility of divides shows a systematic increase from south to north although discussing such a spatial trend was challenging because of the divide bifurcation in Kosado. The cause of this spatially systematic transition of divide mobility in Osado remains unclear. However, as stated in Section 5.1, there appeared to be a few different factors involved in the tectonics of OD1, showing a conspicuous effect of landward tilting on a river profile and a seemingly different direction of divide extension. In addition, the height of the divide is lower in OD1 than those in OD2–3 (Figure 1). The difference in divide mobility may reflect the time lag of the emergence of the island (terrestrialization) and the temporal change in the tectonic mode of tilting although this warrants further scientific investigation and information.

5.3 The Current Location of the Divide in Sado Island

All the identified remnants of stream capture in the present study (Section 4.3) suggest divide migration toward the northwest. This direction is in accordance with that expected from the combination of the tilting direction and stream power law. The distribution of marine terraces and tendency of the river profiles indicate faster uplift on the northwestern side than on the southeast. As noted in the Introduction, SPIM predicts the adjustment of rivers to tectonics, such as short steep profiles in fast-uplifted basins and long gentle profiles in slow-uplifted basins across a divide. To realize this situation for the two adjacent basins under asymmetrical uplift, the divide needs to migrate from the southeast to northwest in the case of Sado Island. The divide migration direction based on the consideration of SPIM with the tilting uplift, therefore, agrees with that suggested by former stream capture. The present Sado, however, shows an unexpected distribution of the river length. Rivers on the northwestern side are longer than those on the southeastern side

 doi:10.20944/preprints202212.0473.v1

(i.e., the divides are located on the southeastern side of the geometric center), as shown in Figures 5, 6, and 7, which is opposite to the SPIM prediction. One potential reason might be that the divide is now at a position that is far from equilibrium, which suggests the notion that the direction of tilting was the opposite to that of the present [19]. If this were true, all the divides would be actively migrating while showing large values of Gilbert metrics, because they have not yet attained their final positions on the northwestern side of the geometrical center; however, in reality, the Gilbert metrics suggest migration only in OD1 and KD2. As the present tilting uplift has continued for at least 300k years [19], it is unlikely that the Gilbert metrics do not reflect modern tectonics owing to being immediately after the beginning of the present tilting uplift.

Even if a stable divide suggested by the Gilbert metrics and $\Delta\chi$ does not imply a state of perfect rest, the migration rate of the divide could possibly be very slow. It seems peculiar that the divide slows down before moving to the northwest across the geometrical center under southeastward tilting uplift, because under such asymmetric uplift, it is conventionally known that the divide should be stable on the northeastern side of the geometric center. This conventionally simple depiction implicitly assumes a finite area for the summation of the two basins. On a continent, the area affected by tilting uplift is usually small relative to the continent, and there are several surrounding competing drainage basins. Therefore, the two adjacent basins in question affected by tilting uplift can be regarded as being confined by surrounding basins, and the summation of the area of the two basins (victim and aggressor) can be assumed to be constant. Sado Island, however, is entirely affected by tilting uplift, and the area of the pair of basins is not confined, but can expand toward the sea.

Although the tilting activities of Osado and Kosado are independent (the axes are not common, as described in Section 2) [17,18], the direction of tilting is similar. As Osado and Kosado are entirely affected by the tilting uplift, the lands are asymmetrically expanded seaward, predominantly on the northwestern rather than on the southeastern coast. Owing to the northwestward land expansion of Osado and Kosado, the geometric center also moves northwestward relative to the divide. Consequently, even if the divide slowly moves northwestward, it is located southeast of the center, as shown in the swath profile (Figure 7). This consideration hold true for all the analysis segments, except for KD4. The basins in KD4 cannot expand their area seaward to the northwest due to the presence of basins in KD3, where these two sections run parallel because of the bifurcation of the divide. (Figures 1 and 7G). Such continuous northwestward expansion of the island, that is, an unconfined situation, appeared to be the primary reason behind the southwestward location of the divides, except for KD4 that is confined to the northwestern side (the faster uplift side) and displays the divide on the northwestern side of the geometric center of its basin.

The present study shows that the position of the drainage divide does not always become stable on the faster uplifted side of the geometric center, but can be in a quasi-equilibrium on the slower uplifted side in the case of unconfined land, even in asymmetric uplifts. The divide of quasi-equilibrium of Sado Island might migrate slowly, but it would be much slower than that of land expanding northwestward and the motion of the geometric center due to asymmetric uplift. The main divides of Sado presumably continued to migrate slowly toward the faster uplifted area (i.e., from southeast to northwest) since the island appeared above sea level, but has never overcome the geometric center. This presumption does not require reverse movement of the tilting uplift, as interpreted in a previous study [19]. To date, there has been no evidence of tectonic inversion of tilting on Sado Island. An interpretation with fewer assumptions would be better (Occam's razor); therefore, the inverse position of the divide relative to tilting uplift should be attributed to land expansion rather than to the reverse of tilting. For a comprehensive understanding of the dynamics of the drainage divide and river network affected by asymmetric uplift, not only confined cases but also unconfined situations should be studied. Therefore, investigations of other study areas under various conditions are required.

 doi:10.20944/preprints202212.0473.v1

6. Conclusions

Rivers and drainages in Sado Island, Japan, were investigated and discussed from the viewpoint of geomorphology, focusing on the divide mobility based on Gilbert metrics and χ parameter, and the following conclusions were obtained.

1. The longitudinal river profiles and the distribution and type of knickpoints reflect southeastward tilting, which accords with the tectonic activity suggested by marine terraces in previous studies.
2. We found abandoned channels which were a result of stream captures and distinctively identified past migration of the drainage divides from southeast to northwest. This migration accords with the direction of the divide migration expected from the stream power incision model, along with the tilting uplift suggested by other geomorphologic characteristics.
3. The standardized delta plots of the Gilbert metrics and $\Delta\chi$ showed the accordance between these two indices, indicating active migration of divides for OD1 and KD2 and 4 as well as inactive divides for OD3 and 4 and KD3. For OD2 and KD1, the plots displayed the disaccord in which the Gilbert metrics suggested the steadiness of divides on local and short-time scales, whereas $\Delta\chi$ implied the divide migration toward the northwest on a long-time scale due to an imbalance between riverine erosion and uplift at the basin scale. The reason for the different states of divides between the sites remains unclear; nevertheless, some features observed in OD1 pointed to the presence of different tectonics (the prominently convex profile and the slightly different direction of the divide extension). The different states of the divides might reflect time and space gaps in landform development inside the island.
4. While the direction of divide migration is comprehensible based on conventional considerations, the present positions of divides in Sado Island are not straightforward, that is, the stable divides are not located on the northwestern side of the geometric center despite southeastward tilting.
5. The apparent anomaly of the divide position in Sado Island can be attributed to the unconfined land area, which is entirely affected by tilting uplift, and it is not necessary to interpret the reverse motion of tilting uplift. A conventional simple consideration of a divide affected by asymmetric uplift, particularly, in a continental case, assumes a fixed geometric center of a constant integrated area of two basins surrounded by many other competing basins that are barely influenced by the asymmetric uplift because of its small spatial range relative to the entire land. However, as most basins on Sado Island face the sea, the area can expand northwestward owing to the southeastward tilting, where the geometric center moves northwestward. The main divides of Sado have continued to migrate toward the northwest since the island had emerged but has never overcome the geometric center.
6. River channels flowing in an unconfined basin tend to show a large disequilibrium, and the dynamics of such non-equilibrium landforms remain to be investigated. Future studies of the drainage divide and river networks affected by asymmetric uplift under various conditions, including not only confined cases but also unconfined situations, are required for a comprehensive understanding of landform dynamics.

Author Contributions:

Conceptualization, A.S and N.E.; methodology, A.S.; validation, A.S.; formal analysis, A.S.; investigation, A.S.; writing—original draft preparation, A.S.; writing—review and editing, A.S. and N.E.; supervision, N.E.; funding acquisition, N.E. All authors have read and agreed to the published version of the manuscript.

Funding: This study was supported by JSPS KAKENHI (Grant Number19K01157).

Acknowledgments: The authors appreciate the developers of the TopoToolbox and Divide Tools, Wolfgang Schwanghart, Adam Forte, and Kelin Whipple. We also thank the following organizations and concerned personnel: The DEM data used in this study were obtained from the Geospatial Information Authority of Japan (GSI: Geographical Survey Institute) (https://www.gsi.go.jp/index.html). The geological map was created modifying AIST's Seamless Geological Map of Japan 1:200,000 V2 (Geological Survey of Japan, AIST, Data updated on April 6, 2020, https://gbank.gsj.jp/seamless/).

Conflicts of Interest: The authors declare no conflict of interest.

References

1. Willett, S.D.; Mccoy, S.W.; Perron, J.T.; Goren, L.; Chen, C.Y. Dynamic reorganization of river basins. *Science* **2014**, *343*, 1248765. https://doi.org/10.1126/science.1248765
2. Goren, L.; Willett, S.D.; Herman, F.; Braun, J. Coupled numerical-analytical approach to landscape evolution modeling. *Earth Surf. Process. Landf.* **2014**, *39*, 522–545. https:// doi.org/10.1002/esp.3514.
3. He, C.; Rao, G.; Yang, R.; Hu, J.; Yao, Q.; Yang, C.J. Divide migration in response to asymmetric uplift: Insights from the Wula Shan horst, North China. *Geomorphology* **2019**, *339*, 44–57. https://doi.org/10.1016/j.geomorph.2019.04.024.
4. Kim, D.-E.; Seong, Y.B.; Weber, J.; Yu, B.Y. Unsteady migration of Taebaek Mountain drainage divide, Cenozoic extensional basin margin, Korean Peninsula. *Geomorphology* **2020**, *352*, 107012. https://doi.org/10.1016/j.geomorph.2019.107012
5. Maneerat, P.; Bürgmann, R. Geomorphic expressions of active tectonics across the Indo-Burma Range. *J. Asian Earth Sci.* **2022**, *223*, 105008. https://doi.org/10.1016/j.jseaes.2021.105008
6. Zhou, C.; Tan, X.; Liu, Y.; Lu, R.; Murphy, M.A.; He, H.; Han Z.; Xu, X. Ongoing westward migration of drainage divides in eastern Tibet, quantified from topographic analysis. *Geomorphology* **2022**, *402*, 108123. https://doi.org/10.1016/j.geomorph.2022.108123
7. Buscher, J.T.; Ascione, A.; Valente, E. Decoding the role of tectonics, incision and lithology on drainage divide migration in the Mt. Alpi region, southern Apennines, Italy. *Geomorphology* **2017**, *276*, 37–50 http://dx.doi.org/10.1016/j.geomorph.2016.10.003
8. Olivetti, V.; Godard, V.; Bellier, O.; ASTER Team. Cenozoic rejuvenation events of Massif Central topography (France): Insights from cosmogenic denudation rates and river profiles. *Earth Planet. Sci. Lett.* **2016,** *444*, 179–191. https://doi.org/10.1016/j.epsl.2016.03.049
9. Zondervan J.R.; Stokes M.; Boulton S.J.; Telfer M.W., Mather A.E. Rock strength and structural controls on fluvial erodibility: Implications for drainage divide mobility in a collisional mountain belt. *Earth Planet. Sci. Lett.* **2020**, *538*, 116221. https://doi.org/10.1016/j.epsl.2020.116221
10. Forte, A.M.; Whipple, K.X.; Cowgill, E. Drainage network reveals patterns and history of active deformation in the eastern Greater Caucasus. *Geosphere* **2015**, *11*, 1343–1364. https://doi.org/10.1130/GES01121.1
11. Shi, F.; Tan, X.; Zhou, C.; Liu, Y. Impact of asymmetric uplift on mountain asymmetry: analytical solution, numerical modeling, and natural examples. *Geomorphology* **2021,** *389*, 107862. https://doi.org/10.1016/j.geomorph.2021.107862.
12. Guerit, L.; Goren, L.; Dominguez, S.; Malavieille, J.; and Castelltort, S. Landscape 'stress' and reorganization from chimaps: Insights from experimental drainage networks in oblique collision setting. *Earth Surf. Process. Landf.* **2018**, *43*, 3152–3163. https://doi.org/10.1002/esp.4477
13. Forte, A.M.; Whipple, K.X. Criteria and tools for determining drainage divide stability. *Earth Planet. Sci. Lett.* **2018**, *493*, 102–117. https://doi.org/10.1016/j.epsl.2018.04.026
14. Li, Z.; Su, Q.; Xie, H.; Wang, B. Geomorphic expression of the Lenglong Ling area, eastern Qilian Shan, and its coupling relationship with the deep structures. *Geol. J.* **2021**, *56*, 3448–3459. https:// doi.org/10.1002/gj.4102
15. Su, Q.; Wang, X.; Lu, H.; Xie, H. Dynamic divide Migration as a Response to Asymmetric Uplift: an example from the Zhongtiao Shan,North China. *Remote Sens*. **2020**, 12, 4188. https://doi.org/10.3390/rs12244188
16. Ye, Y.; Tan, X.; Liu, Y.; Zhou, C.; Shi, F.; Lee, Y.H.; Murphy, M.A. The impact of erosion on fault segmentation in thrust belts: insights from thermochronology and fluvial shear stress analysis (southern Longmen Shan, eastern Tibet). *Geomorphology* **2022**, *397*, 108020. https://doi.org/10.1016/j.geomorph.2021.108020
17. Ota, Y. Coastal terraces of Sado Iland, Japan. *Geogr.Rev.Jpn* **1964**, *37*, 226-242. https://doi.org/10.4157/grj.37.226 (In Japanese with English Abstract)
18. Tamura, A. Holocene marine terrace and crustal movements of Sado Island, Centlal Japan. *Geogr.Rev.Jpn* **1979**, *52-7*, 339-355. https://doi.org/10.4157/grj.52.339 (In Japanese with English Abstract)
19. Ota, Y.; Miyawaki, A.; Shiomi, M. Active Faults on Sado Island, off Cental Japan, and Their Implication on the Marine Terrace Deformation. *J. Geogr (Chigaku Zasshi)* **1992**, *101(3)*, 205–224. (In Japanese with English Abstract) https://doi.org/10.5026/jgeography.101.205
20. Kayahara, K. Geological Map of Niigata Prefecture. *Niigata Prefecture* **1977** (In Japanese)
21. Sugiyama, R. Tertiary igneous activity and its relationship to earth-shell movement. *J. Geogr. (Chigaku Zasshi)* **1956**, *65(3)*, 118–124. https://doi.org/10.5026/jgeography.65.118 (In Japanese)

22. Simazu, M.; Kanai, Y.; Toyama, T.; Ichihashi, K.; Minakawa, J.; Takahama, N. Structural development and igneous activity in the Sado island. *J. Geol. Soc. Jpn.* **1972**, *9*, 147–157. (In Japanese with English Abstract)
23. Okumura, Y.; Miyashita, Y.; Uchide, T. 2019 off Yamagata earthquake and contraction zones along the eastern margin of Japan Sea. *GSJ chishitsu news* **2019**, *8(8)*, 199–203. (In Japanese with English Abstract)
24. Ota, Y.; Matsuda, T.; Naganuma, K. Tilted Marine Terraces of the Ogi Peninsula, Sado Island, Central Japan, Related to the Ogi Earthquake of 1802. J. Seismo. Soc. Jpn. 2nd ser. Zisin. **1976**, *29*, 50–70 (In Japanese with English Abstract)
25. Howard, A.D.; Kerby, G. Channel changes in badlands. *Geol. Soc. Am. Bull.* **1983**, *94(6)*, 739–752. https://doi.org/10.1130/0016-7606(1983)942.0.CO;2.
26. Kirby, E.; Whipple, K.X. Expression of active tectonics in erosional landscapes. *J. Struct. Geol.* **2012**, *44*, 54–75. http://dx.doi.org/10.1016/j.jsg.2012.07.009
27. Wobus, C.; Whipple, K.X.; Kirby, E.; Snyder, N.; Johnson, J.; Spyropolou, K.; Crosby, B.; Sheehan, D. Tectonics from topography: Procedures, promise, and pitfalls. *Spec. Pap. Geol. Soc. Am.* **2006**, *398*, 55–74. http://dx.doi.org/10.1130/2006.2398(04)
28. Whipple, K.X.; Forte, A.M.; Dibiase, R.A.; Gasparini, N.M.; Ouimet, W.B. Timescales of landscape response to divide migration and drainage capture: Implications for the role of divide mobility in landscape evolution. *J. Geophys. Res. Earth Surf.* **2017**, *122*, 248–273. https://doi.org/10.1002/2016jf003973
29. Chen, Y.W.; Shyu, J. B. H., Chang, C.P. Neotectonic characteristics along the eastern flank of the Central Range in the active Taiwan orogen inferred from fluvial channel morphology, *Tectonics* **2015**, *34*, 2249–2270, https://doi.org/10.1002/2014TC003795
30. Li, B.; Zuza, A. V.; Chen, X.; Hu, D.; Shao, Z.; Qi, B.; Wang, Z.; Levy, D. A.; Xiong, X. Cenozoic multi-phase deformation in the Qilian Shan and out-ofsequence development of the northern Tibetan Plateau. *Tectonophysics* **2020**, *782–783*, 228423. https://doi.org/10.1016/j.tecto. 2020.228423
31. Schwanghart, W.; and Scherler, D. Short Communication: TopoToolbox 2-MATLAB-based software for topographic analysis and modeling in Earth surface sciences. *Earth Surf. Dyn.* **2014**, *2*, 1–7, https://doi.org/10.5194/esurf-2-1-2014
32. Schwanghart, W.; and Scherler, D. Bumps in river profiles: uncertainty assessment and smoothing using quantile regression techniques. *Earth Surf. Dyn.* **2017**, 5, 821–839, https://doi.org/10.5194/esurf-5-821-2017,2017
33. Perron, J. T.; Royden, L. An integral approach to bedrock river profile analysis. *Earth Surf. Process. Landf.* **2013**, *38*, 570–576, https://doi.org/10.1002/esp.3302, 2013.
34. Trost, G.; Robl, J.; Hergarten, S.; Neubauer, F. The destiny of orogen-parallel streams in the Eastern Alps: the Salzach–Enns drainage system. *Earth Surf. Dyn.* **2020**, *8*, 69–85. https://doi.org/10.5194/esurf-8-69-2020, 2020.
35. Fan, N.; Kong, P.; Robl, J.C.; Zhou, H.; Wang, X.; Jin, Z.; Liu, X. Timing of river capture in major Yangtze River tributaries: insights from sediment provenance and morphometric indices. *Geomorphology* **2021**, *392*, 107915. https://doi.org/10.1016/j. geomorph.2021.107915
36. Clark, M. K.; Schoenbohm, L. M.; Royden, L. H.; Whipple, K. X.; Burchfiel B. C.; Zhang, X.; Tang, W.; Wang, E.; Chen, L. Surface uplift, tectonics, and erosion of eastern Tibet from large-scale drainage patterns. *Tectonics* **2004**, *23*, TC1006. https://doi.org/10.1029/ 2002TC001402
37. Genno, R.; Endo, N. Adjustment processes of mountainous rivers affected by tilting uplift: Laboratory experiments and a case study of Yakushima Island, Japan. *Island Arc*, **2018**, *28(1)*, e12278. https://doi.org/10.1111/iar.12278
38. Lavé, J.; Avouac, J.P. Fluvial incision and tectonic uplift across the Himalayas of central Nepal. *J. Geophys. Res.* **2001**, *106(Bll)*, 26561–26591. https://doi.org/10.1029/2001JB000359
39. Loget, N.; Davy P.; Van Den Driessche, J. Mesoscale fluvial erosion parameters deduced from modeling the Mediterranean sea level drop during the Messinian (late Miocene). *J. Geophys. Res.* **2006**, *111*, F03005. https://doi.org/10.1029/2005JF000387